# X-Ray Image Contrast from a Simple Phase Object

T. J. Davis,[1] T. E. Gureyev,[1,2] D. Gao,[1] A. W. Stevenson,[1] and S. W. Wilkins[1]

[1]*Division of Materials Science and Technology, Commonwealth Scientific and Industrial Research Organization, Private Bag 33, Rosebank MDC, Clayton, Victoria 3169, Australia*

[2]*School of Physics, University of Melbourne, Parkville, Victoria 3052, Australia*

(Received 14 November 1994)

We report the first x-ray images of a simple phase object using a new technique of differential phase-contrast imaging. The image contrast is obtained by resolving phase gradients in a beam of 0.154 nm x rays using diffraction from a perfect crystal analyzer. The contrast variations in the images are explained using dynamical x-ray diffraction theory.

PACS numbers: 61.10.–i

Although phase-contrast imaging has been used for many years at optical wavelengths, the lack of useful focusing devices has prevented the development of analogous systems for hard x rays ($\lambda < 1$ nm). For soft x rays ($\lambda = 1-4$ nm), phase-contrast imaging has been performed at synchrotron sources using Fresnel lenses [1,2], but specimen thickness is limited. For hard x rays, lensless methods have employed crystal interferometers [3] that coherently split the x-ray wave front and subsequently recombine the components to yield phase images [4]. However, phase gradients across a wave front represent variations in the direction of propagation of the wave that can be resolved with analyzers of high angular sensitivity. Such analyzers in the form of perfect crystals exist for hard x rays and are used routinely for controlling the properties of x-ray beams [5]. Recently, these x-ray systems have been used to resolve refractive index variations in weakly absorbing materials yielding substantial image contrast [6,7]. Since these refractive index variations produce phase gradients, this method has been called x-ray phase-contrast imaging [7]. The method differs from the usual interferometric method in that no reference beam is required. Rather, it is a differential method that relies on the phase difference across the wave front. As yet there has been no quantitative investigation of this method of contrast formation in an object that has no absorption but induces a phase shift, i.e., a phase object. Here we report the first observations of contrast formation in an x-ray image of a simple phase object formed from a nonabsorbing plastic film. The theory of x-ray diffraction in perfect crystals is used to analyze the contrast variations in the x-ray images.

The phase shift acquired by an x-ray beam on passing through a dielectric medium depends on the thickness of the medium and the dielectric susceptibility $\chi$ [8,9],

$$\phi(x,y) = (k/2)\int \chi(x,y,z)\,dz\,, \qquad (1)$$

where $k = 2\pi/\lambda$ is the vacuum wave number and the integration is along the path of the x-ray beam, taken to be the $z$ direction. Following the usual conventions in crystallography, the x-ray $\psi$ is related to the phase $\phi$ by $\psi_i(x) = \psi_0(x)\exp[-ikz - i\phi(x,y)]$, so that $\phi < 0$ represents a phase advance. The factor $\chi/2$ is the deviation from unity of the refractive index of the medium for x rays. Away from absorption edges, the dielectric susceptibility for forward scattering is linearly related to the electron density in the medium [9], so that phase gradients are induced in the wave front by gradients in the integrated electron density.

The phase object we used is a 10 $\mu$m thick plastic film that has negligible absorption. For x rays of wavelength $\lambda = 0.154$ nm, we estimate from (1) that the film introduces a phase shift of about $-\pi/2$ rad which represents a phase advance. A large phase gradient is induced in the x-ray wave front by placing the film so that it only partially intercepts the x-ray beam (Fig. 1). The phase gradient represents local changes in the direction of propagation of the wave that we resolve using Bragg diffraction from the 422 planes of a set of silicon crystals. The crystal surfaces are cut at angles close to the Bragg angle for the 422 reflection. Such asymmetric Bragg reflections modify the size and the divergence of the diffracted beams [10]. The first crystal expands and collimates the x rays from a sealed-tube source, producing a plane wave that passes through the thin plastic film. The analyzer crystal was cut from a monolithic block of silicon and uses

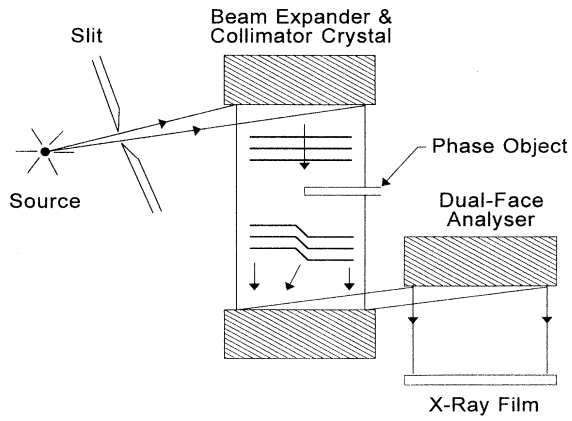


FIG. 1. Sketch of the apparatus showing the phase gradient due to the thin-film phase object.

  

two asymmetric Bragg reflections. The first face of the analyzer has a very narrow angular acceptance (FWHM ~1 arc sec) as a result of the asymmetry and will diffract only those x rays that are incident on it within this angular range. As discussed below, this angular filtering of the x ray waves leads to phase contrast. The degree of contrast in the image of the edge of the film depends on the relative intensities of the waves that are passed by the analyzer. Changing the orientation of the analyzer changes this proportion and alters the contrast. The analyzer also changes the phase of the diffracting waves and this, too, alters the contrast. Because the asymmetric diffraction from the first face spatially condenses the beam, a second crystal face is used to expand the beam to its original size for imaging on the x-ray film.

A series of images of the thin-film phase object was obtained as the analyzer was stepped through the Bragg peak (Fig. 2). The first image [Fig. 2(a)] is a radiograph taken by placing the x-ray film in front of the analyzer crystal. At the upper and lower left of the image are strips of lead tape used to locate the edge of the phase object. The contrast in this image is due to imperfections in the surface of the monochromator crystal. The phase object is not observed, demonstrating that it has negligible absorption. When the x-ray film is placed behind the analyzer, the edge of the phase object is observed as a vertical line running parallel to the edges of the lead tape. As the analyzer is rotated through the Bragg peak, the contrast changes from positive, through zero, to negative [Figs. 2(b), 2(c), and 2(d)]. However, with a further rotation of the analyzer, the contrast becomes positive again. This behavior is associated with the distribution in angle of the plane wave components that make up the phase discontinuity, i.e., it depends on the spatial frequencies of the discontinuity. We also observe that the contrast at the symmetric positions $\Delta\theta = \pm 0.3''$ about the Bragg peak is different [Figs. 2(c) and 2(d)]. Note that the spatial resolution in these images is limited by the divergence of the x rays that result from the finite size of the x-ray source and from the wavelength spread in the beam. In addition, the exposure times increase dramatically as the analyzer is rotated away from the Bragg angle.

The observed variations in contrast can be explained using dynamical diffraction theory. The Bragg diffracted wave from a thick crystal is given as a convolution over the incident wave $\psi_i(x) = \psi_0 \exp[-i\phi(x)]$ at the crystal surface [11]

$$\psi_d(x) = \int_{-\infty}^{\infty} P(Bx')\psi_i(x - x')\, dx', \tag{2}$$

where $P(Bx)$ is the point-spread function of the analyzer crystal, and the $x$ axis lies in the diffraction plane and parallel to the crystal surface. The parameter $1/B$ is the projection onto the $x$ axis of the dynamical extinction distance. The convolution (2) interferes points on the wave front lying within a distance of order $1/B$, so that a localized phase disturbance in the incident wave may enhance or diminish the intensity of the diffracted wave, depending on the relative phase, i.e., the phase gradient, across the wave front.

The variations in contrast are most easily explained in Fourier space where the convolution becomes a simple

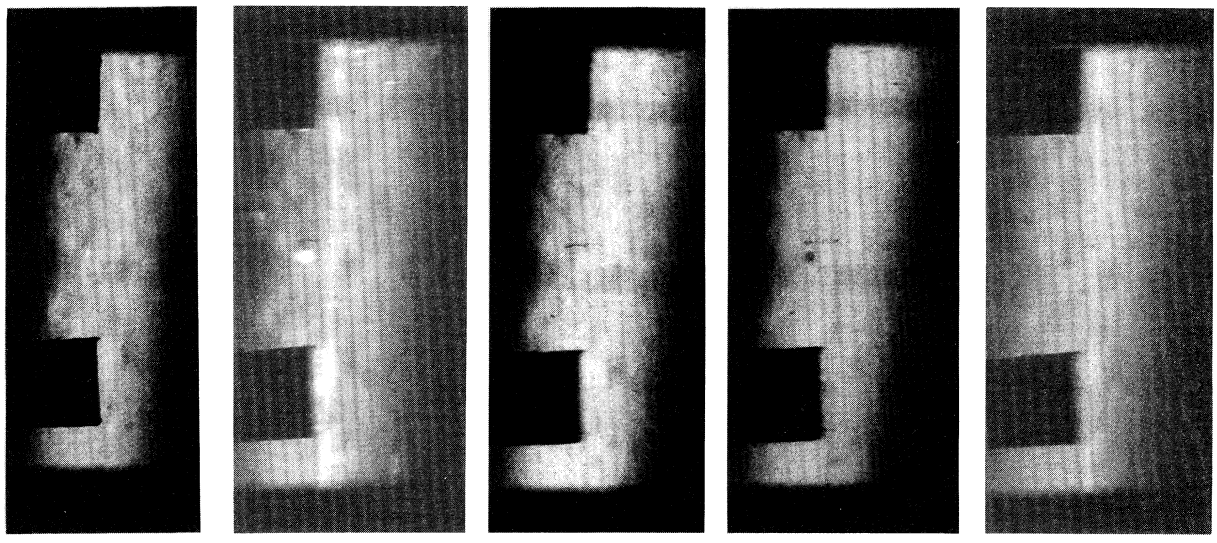


FIG. 2. A radiograph (a) and phase-contrast images for different orientations of the analyzer: (b) $\Delta\theta = -1.2''$, (c) $-0.3''$, (d) $0.3''$, and (e) $0.9''$. The position of the 10 $\mu$m plastic film relates to the left half plane of the image and the film-edge position is marked by a lead strip (opaque). Asymmetric diffraction takes place in the horizontal direction.

product. The Fourier transform of the crystal point-spread function is the crystal reflectance [12] $R(f)$. We use the spatial frequency $f = \Delta\theta/\lambda$ across the incident wave front instead of the angle of incidence relative to the Bragg angle $\Delta\theta$ to emphasize the fact that the analyzer acts as a spatial filter. The spatial filtering properties of perfect crystals are discussed elsewhere [13]. The magnitude and the phase of the reflectance from the first face of the analyzer are shown in Fig. 3(a). The contrast in the images of the phase object results from two separate mechanisms. The first is due to amplitude filtering property of the analyzer that rejects waves with spatial frequencies that do not lie beneath the peak. The second is due to the phase inverting property that shifts by 180° the phases of the waves with spatial frequencies $f < 0$.

The wave from the phase object incident on the analyzer surface can be written in the form

$$\begin{aligned} \psi_i(x) &= 1 + H(x)[\exp[-i\phi] - 1], \\ H(x) &= 0, \quad x < 0 \\ &= 1, \quad x \geq 0, \end{aligned} \tag{3}$$

where the wave passing through the phase object has a unit amplitude and the edge of the phase object is located at $x = 0$. Far from the edge of the phase object, the x-ray wave front remains unperturbed and plane. The Fourier transform of the plane wave is a $\delta$ function that is displaced along the spatial frequency axis as the analyzer crystal is rotated. When the $\delta$ function falls under the peak of the crystal reflectance curve, there is a strong diffracted beam. Away from this region the diffracted beam is weak. The discrete Fourier transform of the incident wave over a region $[-L, L]$ bounding the edge of the phase object is

$$\begin{aligned} \mathcal{F}(\psi_i)(f_n = 0) &= [1 + \exp(-i\phi)]/2, \\ \mathcal{F}(\psi_i)(f_n \neq 0) &= \frac{i}{4\pi f_n L}[1 - \exp(-i\phi)][1 - (-1)^n], \end{aligned} \tag{4}$$

where $f_n = n/2L$, and $n$ is an integer. The envelope of the amplitude (oscillating term omitted for clarity) and the phase of the Fourier transform of the incident wave with $\phi = -\pi/2$ are shown in Fig. 3(b). The phase discontinuity creates a large number of spatial frequencies in the wave front. Each spatial frequency is associated with a plane wave propagating in a direction $\Delta\theta = \lambda f$ with an amplitude that varies as $1/f$.

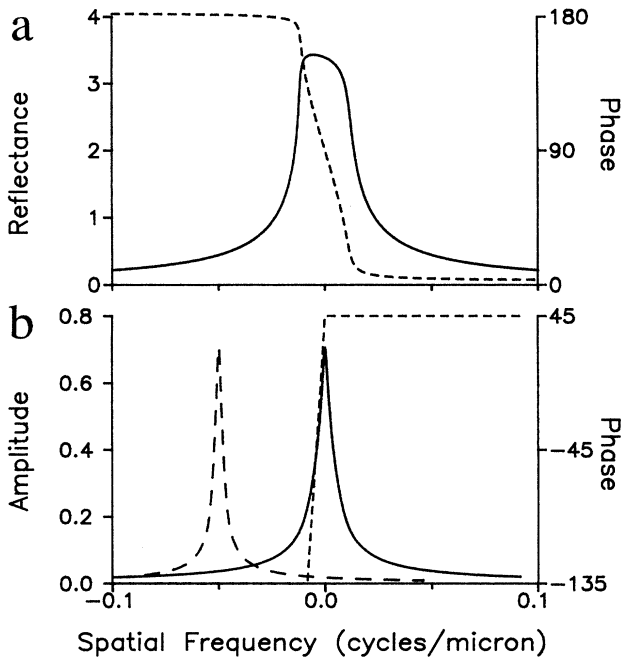


FIG. 3. The magnitude (solid curve) and phase (short-dashed curve) of (a) the analyzer crystal reflectance and (b) the envelope of the Fourier transform of the wave front that has been perturbed by the phase object. The Fourier transform of this wave front is displaced along the spatial frequency axis as the analyzer crystal is rotated (long-dashed curve).

The amplitude filtering property of the analyzer leads to contrast in the following way. At the Bragg angle, the maxima of the Fourier transforms of the unperturbed and perturbed portions of the wave front are beneath the analyzer peak. Because the Fourier spectrum of the perturbed wave front is spread out, some of the Fourier components are greatly diminished by the analyzer so that the intensity relative to the unperturbed wave front is reduced. This produces negative contrast, such as observed in Fig. 2(d). With the analyzer rotated away from the Bragg angle in either direction, the maxima are translated away from the reflectance peak. The $\delta$-function response of the unperturbed wave is greatly diminished. However, some of the Fourier components of the perturbed wave remain under the peak [see long dashed curve in Fig. 3(b)]. Positive contrast will result if the intensity of the components under the peak is greater than the diminished intensity of the unperturbed wave, as observed in Figs. 2(b) and 2(e).

The analyzer crystal also changes the phases of the Fourier components. The phase change varies almost linearly with $f$ in the region about $f = 0$ and leads to phase inversion of the components at $f < 0$ [Fig. 3(a)]. When we inverse Fourier transform, this phase change leads to interference between different Fourier components that enhance the intensity in some regions and diminish the intensity in other regions, changing the contrast. We find that the phase inversion property of the analyzer is responsible for the asymmetric contrast behavior between symmetric settings ($\Delta\theta = \pm 0.3''$) of the analyzer [see Figs. 2(c) and 2(d)]. In some sense, this contrast formation mechanism is similar to that of the interferometric method except that, here, the x-ray wave front acts as its own reference wave. The contrast arises from the interference between regions of the wave front that have different phases. In general, both amplitude filtering and phase

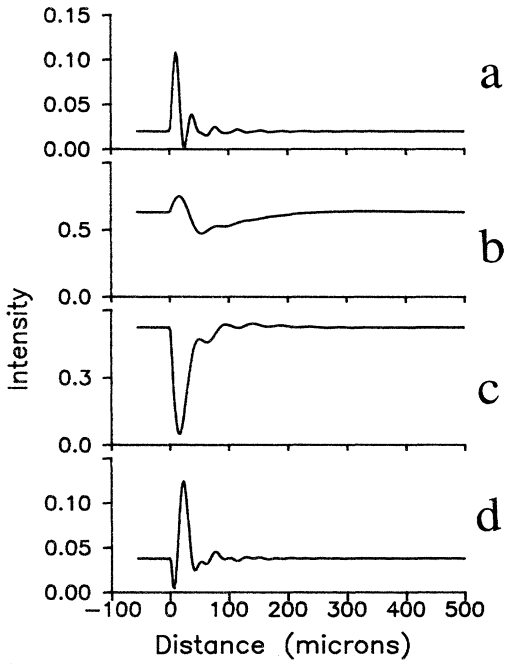


FIG. 4. The diffracted wave profiles from the asymmetric silicon 422 two reflection analyzer calculated for the angles used in the experiments: (a) $\Delta\theta = -1.2''$, (b) $-0.3''$, (c) $0.3''$, and (d) $0.9''$.

inversion will contribute to the formation of contrast in images of phase objects.

The diffracted wave profile across the surface of the analyzer crystal can be calculated from the inverse transform of the product of the crystal reflectance and the transform of the wave (4). The calculated intensity profiles across the images for the analyzer angles corresponding to the experiments (Fig. 4) show qualitative agreement with experiment. Because of instrumental broadening, the low amplitude oscillations in the x-ray profiles are not observed. In general, because of the small angles involved in phase-contrast imaging, high stability apparatus and highly perfect crystals are required. Whether or not phase contrast is observed depends on the magnitude of the phase disturbance and the quality of the instrumentation.

[1] G. Schmahl, D. Rudolph, and P. Guttmann, in *X-Ray Microscopy II,* edited by D. Sayre, M. Howells, J. Kirz, and H. Rarback, Springer Series in Optical Science, Vol. 56 (Springer-Verlag, Berlin, 1988), pp. 228–232.

[2] J. R. Palmer and G. R. Morrison, in *X-Ray Microscopy III,* edited by A. G. Michette, G. R. Morrison, and C. J. Buckley, Springer Series in Optical Science, Vol. 67 (Springer-Verlag, Berlin, 1992), pp. 278–80.

[3] U. Bonse and M. Hart, Appl. Phys. Lett. **6**, 155–156 (1965); Z. Phys. **188**, 154–164 (1965); Acta Cryst. A **24**, 240–245 (1968).

[4] U. Bonse and M. Hart, Appl. Phys. Lett. **7**, 99–100 (1965).

[5] M. Hart, Rep. Prog. Phys. **34**, 435–490 (1971); R. Caciuffo, S. Melone, F. Rustichelli, and A. Boeuf, Phys. Rep. **152**, 1–71 (1987); T. J. Davis, J. X-Ray Sci. Technol. **2**, 180–194 (1990).

[6] N. Mitrofanov, K. Podourets, V. Somenkov, A. Tyugin, P. Chistyakov, and S. Shilshtein, Soviet Patent No. 1402871 (priority 13.11.86); V. A. Somenkov, A. K. Tkalich, and S. S. Shilstein, J. Tech. Phys. **61**, 197–201 (1991); E. A. Belyaevskaya, V. P. Efanov, and V. Ingal, Russian Patent No. 2012872 (priority 14.05.91) and U.S. Patent No. 5319694 (priority 11.12.92); E. A. Beliaevskaya, V. N. Ingal, and P. V. Petrashen, in the Proceedings of the European Symposium on X-Ray Topography and High Resolution Diffraction, Berlin, Germany, 1994 (unpublished), p. 44; V. N. Ingal and E. A. Beliaevskaya, *ibid.* p. 117; A. A. Manushkin, N. L. Mitrofanov, K. M. Podurets, V. A. Somenkov, and S. S. Shilstein, *ibid.* p. 147.

[7] S. W. Wilkins, Australian Patent No. PM0583/93 (1993); T. J. Davis, D. Gao, T. Gureyev, A. W. Stevenson, and S. W. Wilkins, Nature (London) **373**, 595 (1995).

[8] T. J. Davis, Acta Cryst. A **50**, 686–90 (1994).

[9] R. W. James, *The Optical Principles of the Diffraction of X-Rays* (Bell, London, 1948); L. V. Azároff, R. Kaplow, N. Kato, R. J. Weiss, A. J. C. Wilson, and R. A. Young, *X-Ray Diffraction.* (McGraw-Hill, Sydney, 1974), pp. 180–183.

[10] K. Nakayama, H. Hashizume, A. Miyoshi, S. Kikuta, and K. Kohra, Z. Naturforsch. A **28**, 632–638 (1973); T. Matsushita and H. Hashizume, *Handbook on Synchrotron Radiation,* edited by E. E. Koch (North-Holland, Amsterdam, 1983), Vol. 1, Chap. 4.

[11] T. Uragami, J. Phys. Soc. Jpn. **27**, 147–154 (1969); A. M. Afansas'ev and V. G. Kohn, Acta Cryst. A **27**, 421–430 (1971).

[12] Z. G. Pinsker, *Dynamical Scattering of X-Rays in Crystals,* Springer Series in Solid-State Sciences, Vol. 3 (Springer-Verlag, Berlin, 1978), pp. 388–392.

[13] T. J. Davis, CSIRO DMST Internal Report, 1994 (unpublished).

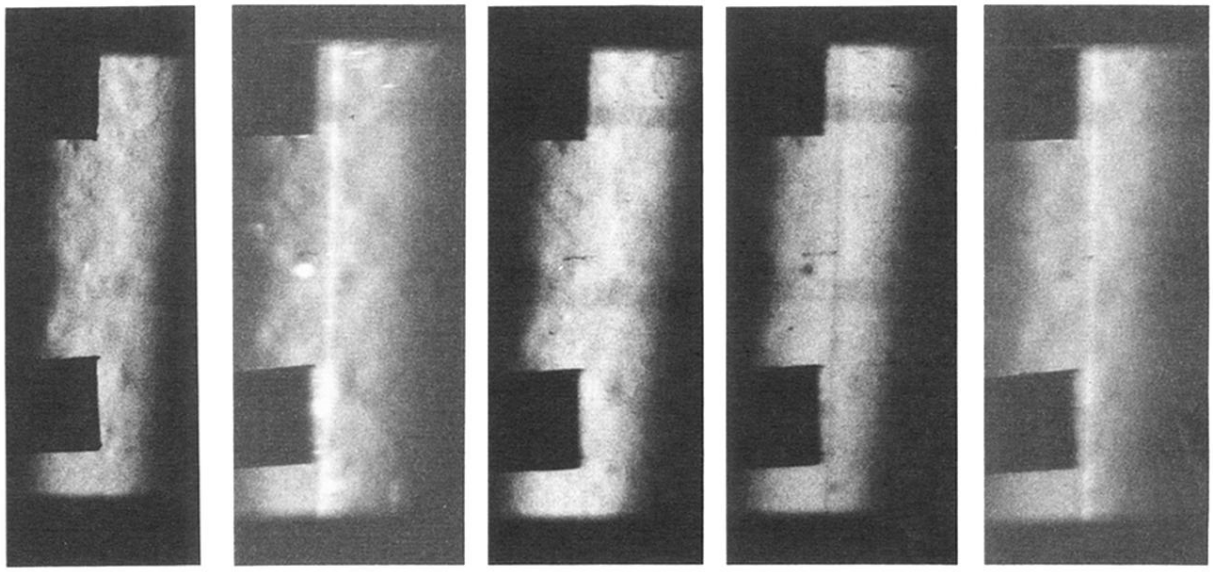


FIG. 2. A radiograph (a) and phase-contrast images for different orientations of the analyzer: (b) $\Delta\theta = -1.2''$, (c) $-0.3''$, (d) $0.3''$, and (e) $0.9''$. The position of the 10 $\mu$m plastic film relates to the left half plane of the image and the film-edge position is marked by a lead strip (opaque). Asymmetric diffraction takes place in the horizontal direction.